Rationalization of solid-state NMR multi-pulse decoupling strategies: Coupling of spin I = ½ and half-integer quadrupolar nuclei

Cassandre Kouvatas[1], Nasima Kanwal[2], Julien Trebosc[3], Claire Roiland[1], Laurent Delevoye[3], Sharon E. Ashbrook[2], Eric Le Fur[1], Laurent Le Pollès[1]

[1] Ecole Nationale Supérieure de Chimie de Rennes, UMR6226, « Institut des Sciences Chimiques de Rennes », 11 allée de Beaulieu, CS 50837, 35708, France
[2] School of Chemistry, EaStCHEM and Centre of Magnetic Resonance, University of St Andrews, St Andrews KY16 9ST, UK
[3] Univ. Lille, CNRS, Centrale Lille, ENSCL, Univ. Artois, UMR 8181 – UCCS – Unité de Catalyse et Chimie du Solide, F-59000 Lille, France

Keywords :
Solid state NMR, Multi-Pulse decoupling, heteronuclear scalar interaction, half integer quadrupolar nucleus, simulations, resolution improvement, characterization of inorganic materials

Highlights :

- Decoupling of heteronuclear scalar interaction between observed ½-spin nucleus and half-integer quadrupolar nuclei
- Case of Multi-Pulse (MP) decoupling scheme
- Study of the influence of intrinsic material parameters (heteronuclear dipolar and J coupling, quadrupolar interaction, spin nature) and instrumental parameters (MAS rate, pulse field strength) on MP decoupling efficiency and enhancement of spectral resolution
- Rationalization of the MP parameterizing and instrumental set up
- Combination of numerical approach and experimental data

Abstract:
In this paper we undertake a study of the decoupling efficiency of the Multiple-Pulse (MP) scheme, and a rationalization of its parameterization and of the choice of instrumental set up. This decoupling scheme is known to remove the broadening of spin-1/2 spectra I, produced by the heteronuclear scalar interaction with a half-integer quadrupolar nucleus S, without reintroducing heteronuclear dipolar interaction. The resulting resolution enhancement depends on the set-up of the length of the series of pulses and delays of the MP, and some intrinsic material and instrumental parameters. Firstly through a numerical approach, this study investigates the influence of the main intrinsic material parameters (heteronuclear dipolar and J coupling, quadrupolar interaction, spin nature) and instrumental parameters (spinning rate, pulse field strength) on efficiency and resolution enhancement of the scalar decoupling scheme. A guideline is then proposed to obtain quickly and easily the best resolution enhancement *via* the rationalization of the instrumental and parameter set up. It is then illustrated and tested through experimental data, probing the efficiency of MP-decoupling set up using this guideline. Various spin

systems were tested (^{31}P-^{51}V in $VOPO_4$, ^{31}P-^{93}Nb in $NbOPO_4$, ^{119}Sn-^{17}O in $Y_2Sn_2O_7$), combined with simulations results.

1. INTRODUCTION

In solid-state NMR spectroscopy, improving the spectral resolution is vital for the detailed structural investigation of solid materials. In particular, homonuclear and heteronuclear decoupling have been widely used to remove the significant dipolar couplings that typically affect NMR spectra of solids, but are removed in solution by rapid molecular tumbling. In recent years, attention has been focused on improving the resolution of NMR spectra of nuclei with spin quantum number I = ½ that are broadened by heteronuclear interactions (such as scalar and dipolar coupling) with highly abundant surrounding nuclei. There are several possible ways to remove these interactions. For example, magic-angle spinning (MAS), where the sample is rotated around an axis inclined at an angle of 54.7° with respect to the external field B_0, leads to a time-dependence of the heteronuclear dipolar coupling, which results in a manifold of spinning sidebands. In addition, the application of radiofrequency (RF) pulses to the coupled heteronucleus during the signal acquisition can be used typically to remove (or in some cases to selectively retain) heteronuclear interactions.

Heteronuclear dipolar-decoupling schemes are commonly employed in solid-state NMR experiments, with the primary aim of improving spectral resolution. Originally employed in solution-state NMR spectroscopy, continuous wave (CW) decoupling [1] is now also routinely used in solid-state NMR MAS. Owing to the limitations of this simple decoupling scheme, a number of more complex decoupling schemes have been specifically developed for use on rotating solids, some using continuous irradiation or adiabatic pulses, including TPPM (and its related variant XiX) [2–4], the SPINAL schemes [5], DFS [6], PISSARO or rCW [7–9] and other approaches [10–14].

The choice of decoupling scheme depends upon the type of heteronuclear interactions that broadens the spectral lines [15,16]. It has been shown that the heteronuclear scalar coupling between nuclei with spin quantum number I = ½ spin and surrounding quadrupolar nuclei (I > 1/2) with half-integer spin quantum number can dramatically decrease the spectral resolution and hinder the extraction of structural and chemical information [16–21]. Although the heteronuclear dipolar coupling can, in principle, be averaged by MAS, the introduction of other time-dependent phenomena, such as RF irradiation (as applied during a decoupling sequence for example), can lead to an interference effect if the two happen on a similar timescale. This can result in an unwanted recoupling of the heteronuclear dipolar interaction, leading to an increased broadening of spectral lines, which is added to the broadening due to the 2nI+1 multiplet that results from the heteronuclear scalar coupling (where n is the number of neighboring quadrupolar nuclei with spin quantum number I).

In recent years, the Rotor Asynchronized – MultiPulse RA-MP decoupling scheme [16] (showed in Fig. 1) has been developed to overcome this problem, and has shown good efficiency for the decoupling of the heteronuclear scalar interaction between a spin I = ½ nucleus and a proximate half-integer quadrupolar nucleus, without reintroducing heteronuclear dipolar coupling. This scheme is based on the application of a series of

moderate strength RF-field pulses (of duration τ_p) spaced by a time interval or "delay" (of duration τ_d), chosen such that $\tau_p + \tau_d \neq \tau_r$, where τ_r is the MAS rotor period. However, the efficiency of this decoupling scheme has been shown to be limited for the case of strong heteronuclear dipolar and scalar couplings or the presence of a large quadrupolar interaction on the coupled spin [20,21]. To date, the RA-MP scheme has not been widely used, despite showing excellent efficiency (often offering significant improvements over CW-based approaches) when employed in the appropriate case. When applicable, this approach requires an appropriate selection of the decoupling parameters (i.e., τ_p and τ_d) with respect to the nature of the nuclei involved in the coupling and the other experimental parameters (i.e., MAS rate and RF field strength) employed, in order to obtain the best possible results.

Here we investigate the influence of instrumental parameters and those parameters intrinsic to the material studied on the MP *decoupling* of the heteronuclear scalar interaction between spin I = ½ nuclei and half-integer quadrupolar nuclei while considering possible *recoupling* of dipolar interaction. Using a combination of simulation and experimental verification we will develop a time-saving guide to the optimum choice of experimental parameters in order to access the best decoupling performance as the nature of the specific system of interest varies.

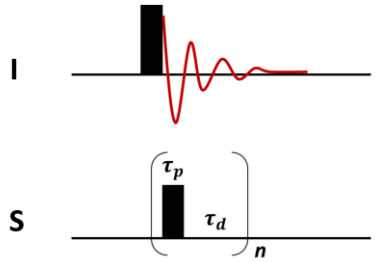

Figure 1 : MP decoupling sequence. The half-integer quadrupolar nucleus S is irradiated by a series of pulses of a duration τ_p, and an interpulse delay τ_d, during signal acquisition on the observed ½ spin nucleus I channel.

2. EXPERIMENTAL METHODS

2.1. Synthesis

2.1.1. γ-$VOPO_4$

γ-$VOPO_4$ was synthesized by thermal decomposition of $VOHPO_4.0.5H_2O$, a precursor that was synthesized according the VPO preparation route [22], by refluxing V_2O_5 in a 90/10 vol mix of isobutanol and benzylic alcohol for 16 h. A stoichiometric amount of phosphoric acid (1 M) was added, followed by one hour of additional reflux. The resulting compound was filtered and washed with a mixture of isobutanol and benzylic alcohol (90/10 ratio), and subsequently dried at 140 °C. The resulting blue powder was recovered and decomposed in air at 750 °C for 5 h. A powder X-ray diffraction pattern obtained for the final yellow powder confirmed the formation of the γ-$VOPO_4$ polymorph [23].

2.1.2. $Y_2Sn_2O_7$

The procedures used for the synthesis and ^{17}O enrichment of $Y_2Sn_2{}^{17}O_7$ can be found in Refs. [24,25].

2.2. Solid-state NMR spectroscopy

2.2.1. γ-$VOPO_4$

^{31}P solid-state NMR experiments were performed using a Bruker Avance III spectrometer equipped with a 14.1 T magnet and a 2.5 mm probehead at Larmor frequencies of 242.938 and 157.852 MHz for ^{31}P and ^{51}V, respectively. ^{31}P experiments were carried out using an RF field strength ν_1^P = 40 kHz (corresponding to a RF pulse duration for a π/2 pulse of 6.25 μs) at a MAS rate of 22 kHz, using a recycle interval of 60 s. Two ^{51}V decoupling strategies were tested during ^{31}P acquisition, using CW and MP schemes. For CW decoupling, the ^{51}V RF field was set to be the highest possible field that could be used without broadening the ^{31}P signals due to the reintroduction of dipolar interaction, *i.e.,* ν_1^V(CW) = 28.8 kHz. Further details for the MP decoupling schemes used are given in the relevant figure captions. Experimental ^{31}P chemical shift scales are shown relative to 1 M H_3PO_4 (aq) at 0 ppm. The RF field strengths used for ^{51}V decoupling were determined using $CsVO_3$ in HCl.

2.2.2. $Y_2Sn_2O_7$

^{119}Sn solid-state NMR experiments were performed using a Bruker Avance III spectrometer equipped with a 9.4 T magnet and a 4 mm triple resonance probehead at Larmor frequencies of 149.115 MHz and 54.243 MHz for ^{119}Sn and ^{17}O, respectively. ^{119}Sn experiments were carried out using an RF field strength ν_1^{Sn} = 100 kHz (corresponding to a RF pulse duration for a π/2 pulse of 2.5 μs) at a MAS rate of 10 kHz, using a recycle interval of 30 s. An RF nutation rate ν_1^O of 35 kHz was used for MP and CW decoupling. ^{119}Sn NMR spectra are shown relative to $(CH_3)_4Sn$ at 0 ppm (measured using a secondary reference of SnO_2 at –604 ppm.

2.3. Density matrix simulations

Numerical density matrix simulations were performed using the SIMPSON program [26]. Considering the computational effort to carry out these simulations, we have considered a two-spin system composed of a spin I = ½ nucleus on the observe channel, and a half-integer quadrupolar nucleus on the decoupled channel. Our simulations were close to those obtained with a three-spin system, validating our two-spin approach. The two nuclei were coupled through both heteronuclear dipolar and isotropic scalar couplings. The simulations included both first- and second-order quadrupolar interactions on the coupled spin. The FIDs were Fourier transformed using 10 Hz apodization and the maximum intensity of the corresponding spectra were used in subsequent plots. The number of gamma angles was set to 19. Testing of several sets of Euler angles were conducted, but their influence is not significant on the results. By comparing simulations carried out with and without considering anisotropy, the results obtained were very close. As a consequence, we did not take into account the CSA interaction in the numerical approach, as its effect is considered as negligible. Other simulation parameters are given in the relevant figure captions.

3. RESULTS AND DISCUSSION

The conditions required for optimum MP performance as the system and experimental parameters varied were considered using both numerical simulation and experimental verification. The effect of varying the magnitude of the quadrupolar coupling, heteronuclear scalar and dipolar interactions, and the influence of instrumental and acquisition parameters such as the decoupling RF field and the MAS rate have been investigated systematically. In the following, we have considered the signal intensity (obtained in simulation or experimentally) as a reliable reflection of the decoupling efficiency.

3.1. Numerical approach

- ***Large quadrupolar coupling and large heteronuclear dipolar interaction***

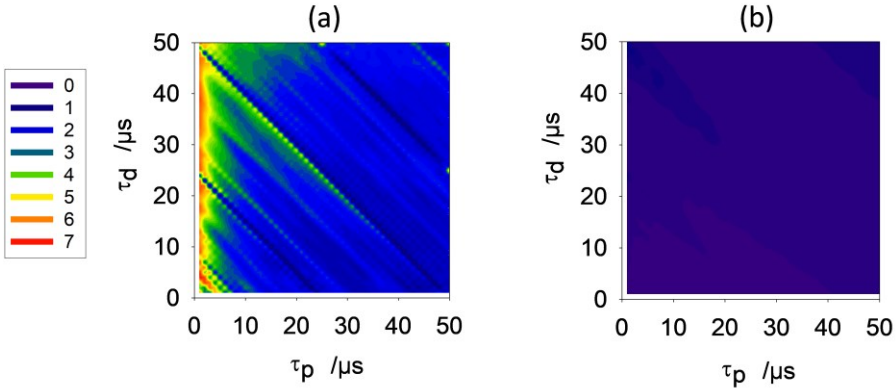

Figure 2 : Two-dimensional contour plots showing the variation in the ^{1}H NMR signal amplitude (obtained from a SIMPSON simulation) under ^{27}Al MP decoupling, as a function of τ_p and τ_d. Decoupling RF field strengths are set to (a) ν_1^{Al} = 2 kHz and (b) ν_1^{Al} = 70 kHz, with ^{27}Al C_Q = 15 MHz and η_Q = 0. Heteronuclear dipolar and scalar couplings were set to 9300 Hz and 375 Hz, respectively. The MAS rate was 20 kHz. The parameters τ_p and τ_d were varied from 0 to 50 μs in steps of 1 μs.

Figure 2 shows the calculated amplitude of the ^{1}H NMR signal under ^{27}Al decoupling, as a function of the decoupling sequence parameters τ_p and τ_d values, at two different decoupling RF field strengths (2 and 70 kHz for Figs. 2a and 2b, respectively). The SIMPSON simulations were performed using the ^{1}H and ^{27}Al spin system parameters typical of aluminum hydride species grafted on γ-alumina [21]. In this system, the ^{1}H/^{27}Al pairs are constrained to the surface, leading to large values of the quadrupolar and dipolar couplings (C_Q = 15 MHz, D_{IS} = –9.3 kHz, J = 375 Hz). Experimentally the ^{1}H sextet resulting from the scalar coupling to ^{27}Al (I = 5/2) shows an asymmetry, due to the presence of both a large heteronuclear dipolar interaction and the significant quadrupolar coupling. The second-order dipolar/quadrupolar cross term that results in this case is significant, and the scalar

interaction cannot be removed simply by MP decoupling used directly during the acquisition. The cross-term interaction is not considered in the simulation, and so to facilitate later comparison. A *J*-HMQC filter was employed prior to the ^{27}Al MP decoupling to efficiently filter the couplings with the ^{27}Al outermost satellite transitions. This leads to a doublet in the ^{1}H NMR spectrum arising from the coupling with only the ^{27}Al central transition. In this situation, ^{27}Al MP decoupling was then used in acquisition to suppress the residual scalar coupling.

The SIMPSON simulations (Fig. 2b) carried out with the set of parameters extracted from the study of Mazoyer *et al*. [21] shows a very low ^{1}H signal amplitude under ^{27}Al decoupling (ν_1^{Al}= 70 kHz), at all conditions considered. This can be explained by the strong recoupling of heteronuclear dipolar interaction observed for large dipolar couplings (-9.3 kHz in this case). At the lower decoupling RF field (ν_1^{Al} = 2 kHz, Fig. 2a), the simulated ^{1}H NMR signal amplitude is low, unless short pulse durations (τ_p = 3-5 µs) are used, again a result of the strong heteronuclear dipolar recoupling. This recoupling decreases dramatically the MP decoupling efficiency, making this scheme as poorly effective to decouple scalar coupling as the CW in that case. Moreover, in the regions where calculated amplitude is the highest (τ_p < 3 µs), the corresponding simulated ^{1}H MAS NMR spectra still show the ^{1}H-^{27}Al *J*-multiplet corresponding to the heteronuclear scalar coupling (Fig. 1 SI 2). These calculations show the inefficiency of MP decoupling in the case of a large heteronuclear dipolar interaction (revealed here through the large second-order cross terms) in agreement with the results obtained by Mazoyer *et al* [21]. Similarly, as in the case of CW decoupling, the MP scheme is not favored for the case of a large dipolar coupling.
However, when associated with a preliminary pulse sequence to filter out the couplings with satellite transitions, MP decoupling outperforms CW [21]. The combination of RA-MP with filtering techniques to remove the effect of satellite transitions will not be discussed any further in this article.

- ***Influence of MAS rate and decoupling RF field strength***

Figure 3 shows the calculated intensities of the ^{31}P NMR signal under different ^{51}V MP decoupling conditions, as a function of pulse lengths, τ_p, and interpulse delay, τ_d. The simulations were carried out considering a ^{51}V – ^{31}P spin system with a ^{51}V (I = 7/2) quadrupolar coupling constant of 3 MHz, typical of that found in $VOPO_4$ materials (usually between 0.5 and 4 MHz) [27–29], together with a *J* coupling of 30 Hz, and a dipolar coupling constant of -396 Hz (calculated for an internuclear distance of 3.18 Å). The simulations were performed with increasing RF field strengths and at two different spinning rates, the two most important experimental parameters to consider. Their influence on the decoupling efficiency can be evaluated together with the influence of the quadrupolar coupling (parameterized using either C_Q or ν_Q) through the adiabatic passage parameter α, described by Grey and Vega [30,31]. The parameter $\alpha = \frac{\nu_1^2}{\nu_r \times \nu_Q}$, where ν_1 is the decoupling RF field strength, ν_r the spinning rate and ν_Q the quadrupolar frequency of the half-integer quadrupolar nucleus (defined in this case as $\nu_Q = \frac{3C_Q}{2I(2I-1)}$). When α >>1, the regime is considered as adiabatic, *i.e.*, the population transfer is facilitated, and a direct consequence is that the reintroduction of dipolar coupling is facilitated as well, as it is in the TRAPDOR sequence [31]. In contrast, when α << 1, the regime is considered sudden (*i.e.*, not in favored

of dipolar recoupling). In the following figures, we have considered different cases with increasing α, ranging from 0.1 to 4.8.

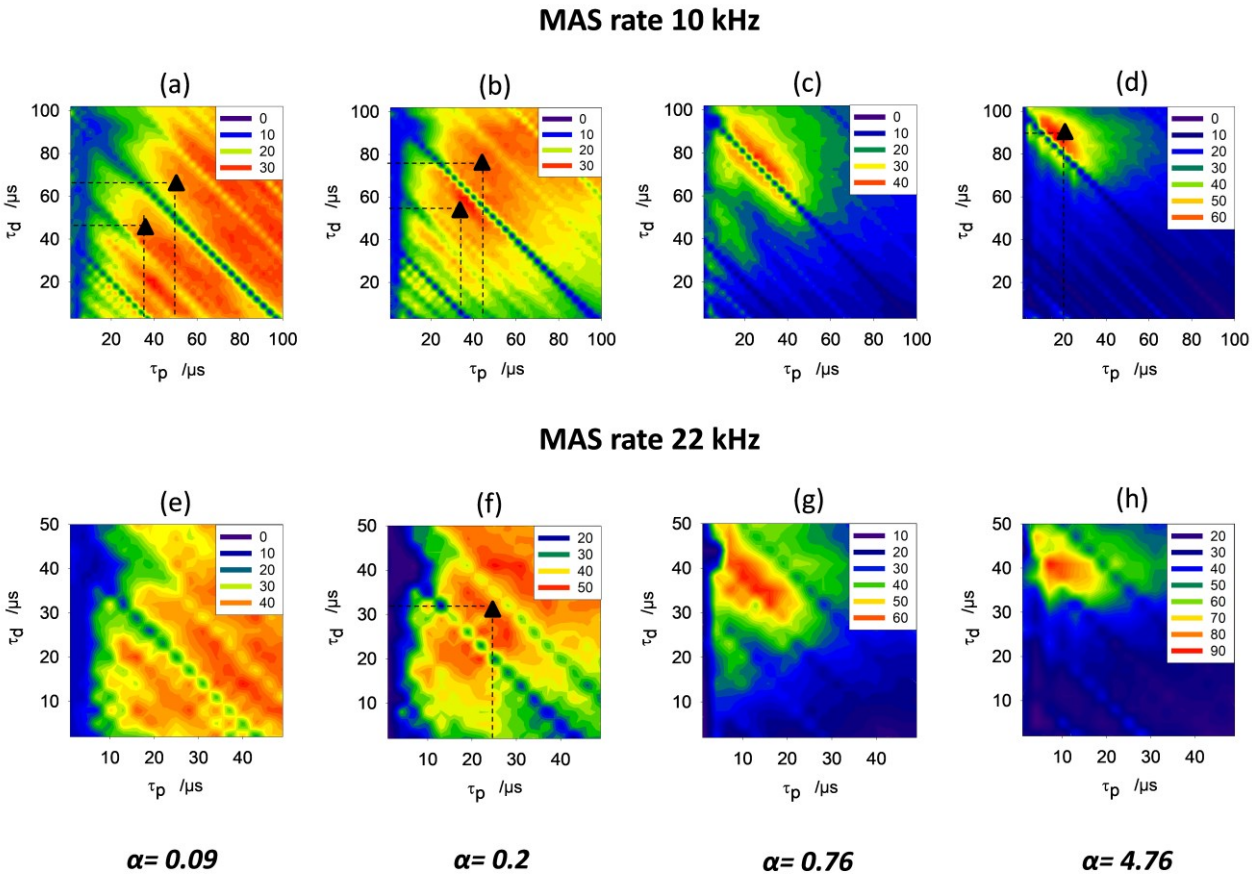

Figure 3 : Two-dimensional contour plots showing the variation in the ^{31}P signal amplitude (obtained from a SIMPSON simulation) under ^{51}V MP decoupling, as a function of τ_p and τ_d. The quadrupolar coupling constant, C_Q, was set to 3 MHz and the asymmetry parameter η_Q to 0. The dipolar and scalar coupling constants were set to -396 Hz and 30 Hz, respectively. Several decoupling RF field were tested for two different MAS rates. Decoupling field strengths of (a) ν_1^{Al} = 14 kHz, (b) ν_1^{Al} = 20.7 kHz, (c) ν_1^{Al} = 40.4 kHz and (d) ν_1^{Al} = 101 kHz were used for an MAS rate of 10 kHz. Decoupling field strengths of (e) ν_1^{Al} = 21.7 kHz, (f) ν_1^{Al} = 30 kHz, (g) ν_1^{Al} = 60 kHz and (h) ν_1^{Al} = 150 kHz were used for an MAS rate of 22 kHz. The adiabatic passage parameter α is (a, e) 0.09 (b, f), 0.2 (c, g), 0.76 and (d, h) 4.76. The parameters τ_p and τ_d were varied in steps of 3 μs. The triangles represent (τ_p,τ_d) pairs of (50 μs, 35 μs) and (60 μs, 60 μs) in Fig 2a, (35 μs, 55 μs) and (45 μs,75 μs) in Fig. 2b, (20 μs, 90 μs) in Fig. 2d, and (24 μs, 32 μs) in Fig. 2f.

Figure 3a shows the amplitude of the ^{31}P NMR signal intensity as a function of (τ_p, τ_d) for a RF field strength of 14 kHz, corresponding to an α value of 0.09. As previously observed [16], the rotor synchronized condition (*i.e.*, $\tau_p + \tau_d = \tau_r$) should be avoided as it leads to a minimum intensity (*i.e.*, poor decoupling performance). However, significant regions of efficient decoupling of heteronuclear scalar interaction on either side of this rotor synchronized condition are observed, making the choice of (τ_p, τ_d) pair straightforward. For example, the (50 μs, 35 μs) or (60 μs, 60 μs) pairs, highlighted with triangles in Fig. 3a, produce similarly good efficiencies of the ^{51}V MP decoupling of ^{31}P-^{51}V scalar interaction. Indeed, when α is small *(i.e.*, a large quadrupolar coupling constant or low RF field strength), the decoupling pulses do not generate a reintroduction of dipolar interaction, with the result that MP and

CW schemes should show similar efficiencies (this is later in this article supported by experimental data). When the decoupling RF field strength is increased (Fig. 3b), the regions that correspond to maximum decoupling efficiencies move towards shorter pulse lengths and longer interpulse delays, although still close to the rotor synchronized condition. For example, in Fig. 3b (α = 0.2), a maximum efficiency is found for (τ_p, τ_d) of (35 µs, 55 µs). The (τ_p, τ_d) pair of (45 µs,75 µs) gives similarly good efficiency. This regime is characterized by an interpulse delay that is always larger than the pulse duration. For larger α parameters (*e.g.*, 0.76 and 4.76 in Figs. 3c and 3d), the maximum efficiency is found towards shorter pulse durations, with a reduced region of efficiency found around the rotor synchronized condition. At α = 4.76, maximum efficiency is obtained for τ_p = 20 µs and τ_d = 90 µs. Any slight variation from this (τ_p, τ_d) pair results in a dramatic loss of MP decoupling efficiency. Finally, increasing the decoupling RF field strength is always favorable in terms of maximum decoupling efficiency. For example, the maximum calculated amplitude for Figs. 3a and 3d are 25 and 60 (arbitrary units), respectively. For a higher MAS rate of 22 kHz (Figs. 3e to 3h), a similar general trend is observed, *i.e.*, shorter τ_p and longer τ_d are favoured as the decoupling RF field strength (and, concomitantly, α) increases. However, the regions corresponding to maximum intensity are larger, leading to a MP decoupling efficiency that is less dependent on the choice of (τ_p, τ_d).

Finally, it can be noted that the maximum calculated amplitude increases with increasing decoupling RF field strength for a given spinning rate, but also increases with increasing spinning rate for a given α parameter. This is illustrated in Fig. 2 SI where simulated ^{27}Al MAS NMR spectra are shown for conditions shown by the triangles in Fig. 3.

- ***Competition effect between heteronuclear scalar and dipolar coupling***

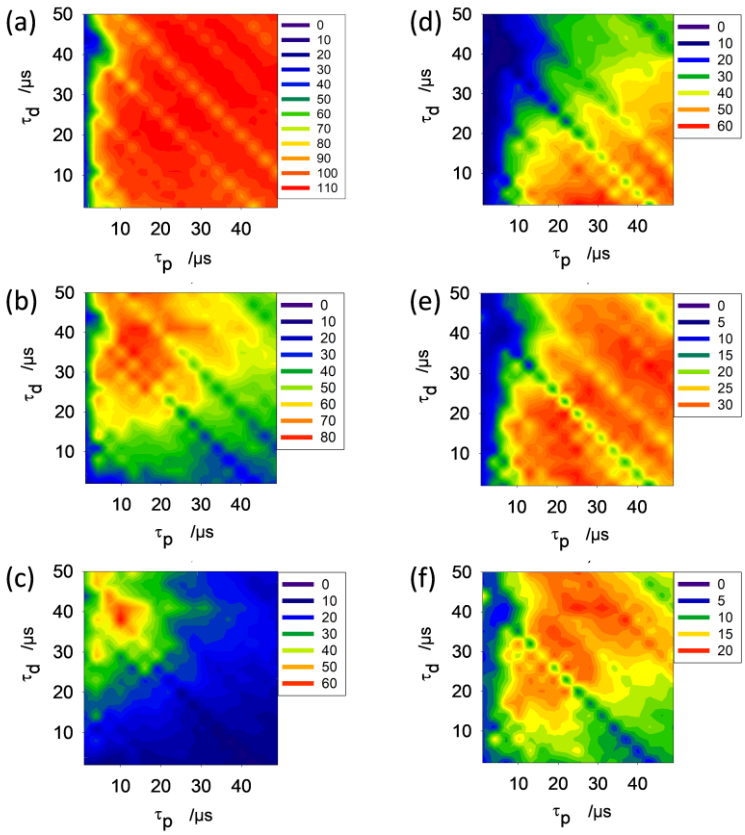

Figure 4 : Two-dimensional contour plots showing the variation in the ^{31}P NMR signal amplitude (obtained from a SIMPSON simulation) under ^{51}V MP decoupling, as a function of τ_p and τ_d. These parameters were both incremented in steps of 3 μs. The quadrupolar coupling constant C_Q was set to 3 MHz and asymmetry parameter η_Q to 0. The decoupling RF field strength was set to ν_1^V = 30 kHz and the MAS rate to 22 kHz. Two scalar coupling constants of (a-c) J_{IS} = 10 Hz and (d-f) J_{IS} = 50 Hz were considered with dipolar coupling constants of (a, d) D_{IS} = –100 Hz, (b, e), –400 Hz and (c, f) –800 Hz. The adiabatic passage parameter α = 0.2.

Figure 4 shows the influence of both the scalar and dipolar coupling constants on the efficiency of the MP decoupling for different values of (τ_p, τ_d). The simulations were performed by considering a spin pair, ^{51}V-^{31}P, with a ^{51}V quadrupolar coupling constant C_Q, that corresponds to the upper value (C_Q = 3 MHz) of those encountered in vanadophosphates.

For a small scalar coupling constant of 10 Hz with a small dipolar coupling (–100 Hz, corresponding to an internuclear distance of 5 Å), most (τ_p, τ_d) pairs provide efficient decoupling of the heteronuclear scalar interaction (as shown in Fig. 4a). This means that no dipolar recoupling occurs and the weak scalar interaction can be easily decoupled. As the dipolar coupling increases (from top to bottom in Fig. 4), the region that corresponds to maximum decoupling efficiency moves towards shorter τ_p and longer τ_d values, on either side of the rotor synchronized condition, *i.e.*, the use of longer τ_p, where the dipolar recoupling would dominate, should be avoided.

For the larger scalar coupling constant of 50 Hz and for a weak dipolar coupling (100 Hz, Fig. 4d), the overall intensity (and therefore MP decoupling efficiency) is significantly reduced with respect to that obtained when J = 10 Hz, and region corresponding to optimum efficiency moves towards longer τ_p values, still ensuring that rotor synchronization is avoided. This illustrates that larger scalar couplings require longer pulse lengths for optimum

MP decoupling. However, when the dipolar coupling is increased, dipolar interaction is reintroduced for long τ_p, such that the signal amplitude decreases rapidly and the pulse lengths for optimum MP decoupling performance tend to decrease. This dependence illustrates the competitive effect of scalar decoupling and reintroduction of dipolar interaction, which has been clearly observed in the case of CW [19] but can also occur for MP.

3.2. Experimental results

The conclusions about the influence of the various experimental and system parameters on MP decoupling efficiency determined from the simulations were tested experimentally on systems containing a spin I = ½ nucleus (^{31}P or ^{119}Sn) J-coupled to a quadrupolar nucleus (^{51}V, ^{93}Nb or ^{17}O).

- **γ-$VOPO_4$: Small C_Q and moderate ^{31}P-^{51}V scalar and dipolar interactions**

Figure 5 compares experimental (Fig. 5a) and calculated (Fig. 5b) ^{31}P signal amplitude under ^{51}V MP decoupling for different (τ_p, τ_d) values. The γ-$VOPO_4$ polymorph was used for the experimental measurements, while calculations were performed using the corresponding NMR and structural parameters [23,29]. The γ-$VOPO_4$ polymorph exhibits a moderate dipolar coupling of –396 Hz (corresponding to a internuclear P-V distance of 3.18 Å), and a small quadrupolar coupling constant, C_Q, of 1.5 MHz, shown above to be favorable for MP decoupling. The experimental and calculated contour plots show good agreement, with similar regions of decoupling efficiency located at pulse lengths slightly shorter than the interpulse delays, on either side of the rotor synchronized condition. This is typical of behavior expected in the intermediate regime (here, α = 0.35), as shown in Fig. 2.

The resolution enhancement provided by MP decoupling was evaluated by comparing the experimental ^{31}P MAS NMR spectrum obtained with MP decoupling (Fig. 5c), with τ_p = 15 μs and τ_d = 37 μs (corresponding to the circle in Fig. 5b), with a spectrum acquired using optimized CW scheme (Fig. 5d) and a final spectrum recorded without decoupling (Fig. 5e). The spectrum acquired without decoupling exhibits two major, broad signals centered at –16.7 and –20.73 ppm (FWHM around 900 and 695 Hz, respectively). The use of (optimized) CW decoupling slightly improves the resolution, and allows the two signals overlapping at –16.7 ppm to be distinguished. However, the spectrum acquired using ^{51}V MP decoupling shows the most spectacular improvement in resolution, enabling the unambiguous assignment of three ^{31}P signals at –20.76, –17.43, and –15.83 ppm. Another signal, belonging to a small impurity of the β-$VOPO_4$ polymorph is observed at –10.59 ppm.

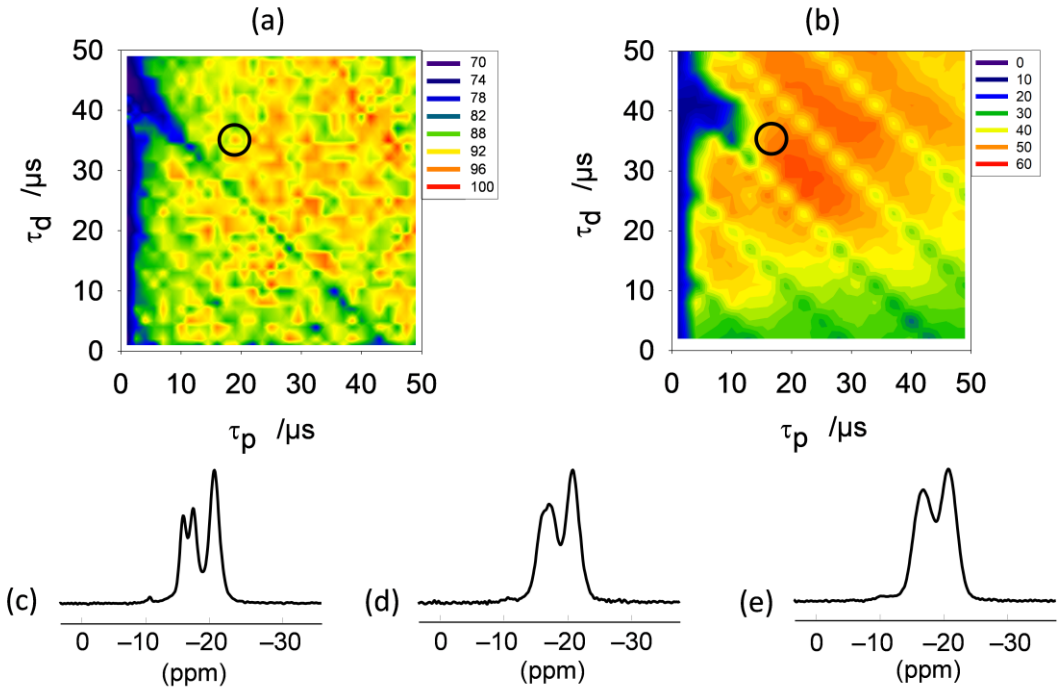

Figure 5 : Two-dimensional contour plots showing the variation in the ^{31}P NMR signal amplitude, and experimental 1D ^{31}P MAS NMR spectra. These plots are obtained (a) in experiment and (b) from a SIMPSON simulation, under ^{51}V MP decoupling, as a function of τ_p and τ_d. The decoupling RF field strength was ν_1^V = 28.8 kHz and the MAS rate was 22 kHz. Experimental data were obtained for the γ-$VOPO_4$ polymorph, and is shown for the ^{31}P site at –22.7 ppm. Simulations were carried out using the spin system parameters extracted from the published data [23,29]: C_Q = 1.5 MHz (ν_Q = 107.1 kHz), η_Q = 0.5 ; δ_{aniso} = –942 ppm ; η_σ = 0.07; D_{IS} = –396 Hz, J_{IS} = 30 Hz. (τ_p, τ_d) steps were (1.5 μs, 1.5 μs) and (3 μs,3 μs) for experimental and simulated plots, respectively. Experimental ^{31}P MAS NMR spectra of the γ-$VOPO_4$ phase were acquired at B_0 = 14.1 T, at an MAS rate of 22 kHz (c) under MP decoupling (ν_1^V = 28.8 kHz), with (τ_P, τ_d) = (15 μs, 37 μs) corresponding to the circles in (a) and (b); (d) with optimized CW decoupling (ν_1^V = 28.8 kHz) and (e) without decoupling. At these conditions, the adiabatic passage parameter, α, is 0.35.

The best fit simulations of the three spectra in Figs. 5c, 5d and 5e are shown in the supplementary information (Fig. 4 SI), together with a table summarizing the fitting results (Table 1 SI). The analytical fits of each spectrum show that the relative integrated intensities of the three ^{31}P signals at –20.76, –17.43, and –15.83 ppm, are approximately 50%, 30% and 20%, respectively (isotropic chemical shifts are determined using the fit of MP decoupled ^{31}P spectrum in Fig. 5c, then rightly adjusted as such for all best-fit simulations). The lowest linewidth is found for the MP decoupled spectrum. Indeed, for the signal at –20.76 ppm, the linewidth decreases by 38%, from 695 Hz (when no decoupling is applied) to 430 Hz (when MP decoupling is used). CW also gives a lower linewidth (573 Hz) for this site (corresponding to a decrease of 18%). The CW scheme used here employs a decoupling RF field optimized to be just lower than that which would reintroduce the dipolar coupling, which means that the resolution enhancement using this approach has reached its limit. Thus, for the same decoupling RF field of 28.8 kHz, the analytical fits show that MP is more efficient for decoupling the heteronuclear scalar interaction than the CW approach.

- **$NbOPO_4$: High C_Q and moderate ^{31}P-^{93}Nb scalar and dipolar interactions**

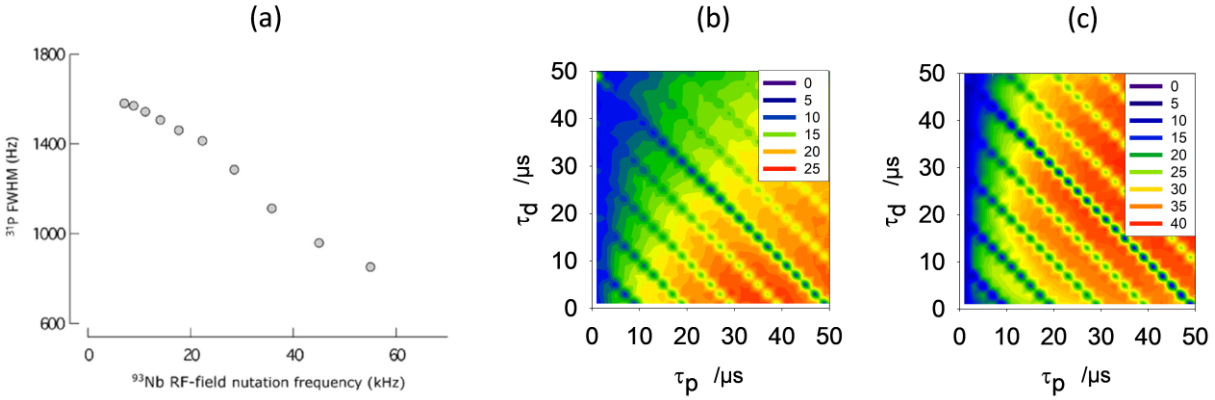

Figure 6 : Two-dimensional contour plots showing the variation in the ^{31}P NMR signal amplitude. (a) ^{31}P linewidth (FWHM in Hz) of the ^{31}P MAS NMR spectrum of $NbOPO_4$ acquired under ^{93}Nb CW decoupling, as a function of the ^{93}Nb decoupling RF field strength, at B_0 = 18.8 T and an MAS rate of 20 kHz. Fig. 6a is extracted with permission[1] from [20], (b, c) Two-dimensional contour plots showing the variation in the ^{31}P NMR signal amplitude, obtained from a SIMPSON simulation, under ^{93}Nb MP decoupling, as a function of τ_p and τ_d. Simulations were conducted with typical spin system parameters for $NbOPO_4$ (C_Q = 21 MHz (ν_Q = 875 kHz), scalar coupling of 40 Hz, dipolar coupling of –304 Hz [20,32]), at an MAS rate of 20 kHz, with (b) ν_1^{Nb} =30 kHz and (c) ν_1^{Nb} = 55 kHz. The adiabatic passage parameter α is (a) 0.05 and (b) 0.18.

Figure 6a shows the ^{31}P linewidth extracted from a ^{31}P MAS NMR spectrum of $NbOPO_4$ as a function of the ^{93}Nb CW decoupling RF field [20]. It is clear that there is a decrease in linewidth as the RF field increases. However, as described by Girard et *al.*, even at the maximum available RF field strength of 55 kHz, the ^{31}P signal linewidth is still decreasing. In other words, under these conditions there is no apparent effect of dipolar recoupling which usually broadens the signal, as was observed in aluminophosphates [16]. This could be explained by the magnitude of the ^{93}Nb quadrupolar coupling (C_Q = 21 MHz), which considerably reduces the recoupling of the heteronuclear dipolar interaction [30,31].

Figs. 6b and 6c show the ^{31}P signal amplitude determined from a SIMPSON simulation under ^{93}Nb MP decoupling, as a function of (τ_p, τ_d), for a spin system similar to $NbOPO_4$, *i.e.,* D_{IS} = –304 Hz (calculated from the structure of Longo *et al.* [32]), C_Q = 21 MHz, J = 40 Hz. Two decoupling RF field strengths were tested: 30 kHz and 55 kHz in Figs. 6b and 6c, respectively. In the simulation the instrumental parameters were set to be comparable to those used in the ^{31}P NMR study of $NbOPO_4$ by Girard *et al.*[20] (*i.e.*, ^{93}Nb decoupling RF field of 55 kHz, MAS rate of 20 kHz, B_0 = 18.8 T). For these settings, the two-dimensional contour plot simulated for a decoupling RF field strength of 30 kHz (Fig. 6b) shows regions of good decoupling efficiency located at rather long pulse lengths, largely at values that are longer than the interpulse delays. This behavior is quite similar to that observed for the CW scheme, and is in agreement with the observations of Girard *et al*. In the particular case where the quadrupolar coupling is large relative to ν_1^2/ν_r, CW may sometimes be better than the MP decoupling scheme. For the higher decoupling RF field of 55 kHz (Fig. 6c), MP could prove useful, as the plot shows areas of higher decoupling efficiency and these are observed

[1] Reprinted from Solid State Nuclear Magnetic Resonance, 84 (6), G. Girard, F. Vasconcelos, L. Montagne, L. Delevoye), ^{31}P MAS NMR spectroscopy with ^{93}Nb decoupling and DFTcalculations: A structural characterization of defects in a niobium-phosphate phase, 210-215, Copyright (2017), with permission from Elsevier.

for wider ranges of τ_p and τ_d. This is an intermediate situation where MP scheme becomes more efficient than CW owing to the increased dipolar recoupling which occurs for CW (in this case) at rather high decoupling RF field due to large quadrupolar coupling.

- **$Y_2Sn_2O_7$: Moderate C_Q and dipolar interaction with high scalar coupling.**

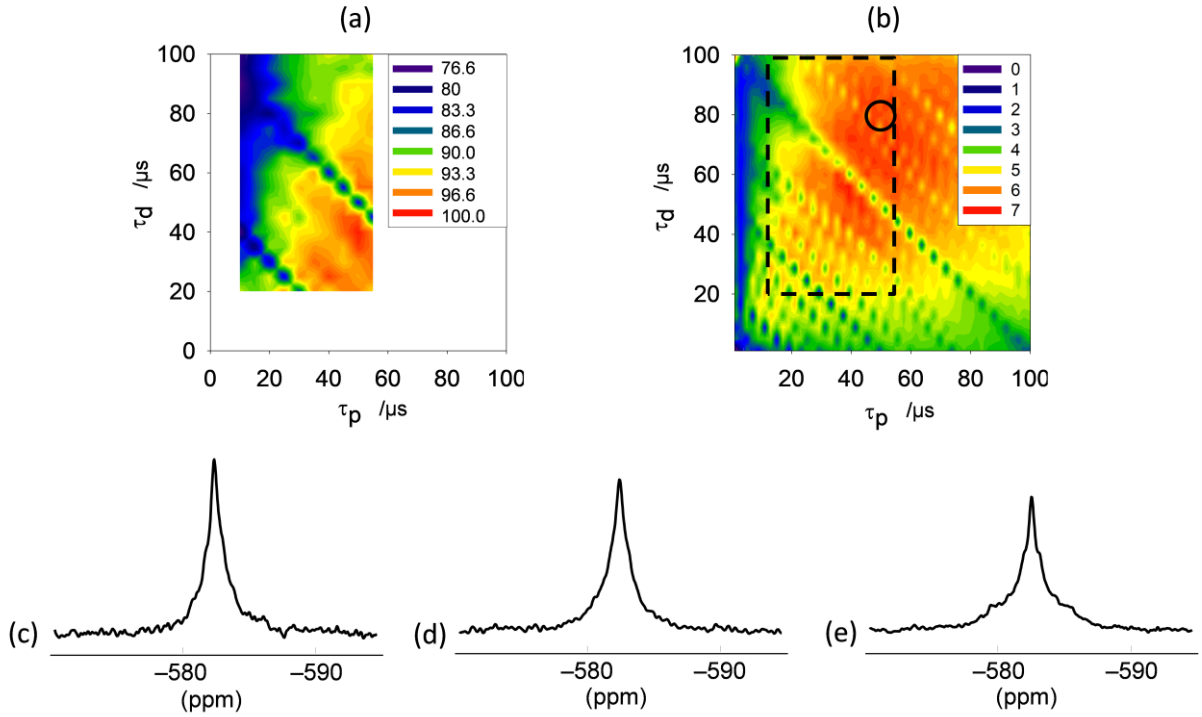

Figure 7 : Two-dimensional contour plots showing the variation in the ^{119}Sn NMR signal amplitude. These plots are obtained (a) in experiment and (b) from a SIMPSON simulation, under ^{17}O MP decoupling, as a function of τ_p and τ_d. Experimental data were obtained for $Y_2Sn_2O_7$, and peak heights are shown for the ^{119}Sn signal at –582.5 ppm. Simulations were carried out using the spin system parameters extracted from the published available data [12], and by the best fit simulation (Fig. 6 SI): C_Q = 4 MHz (ν_Q = 600 kHz), η_Q = 0; η_σ = 0, δ_{aniso} = 0 ppm; D_{IS} = –680 Hz, J_{IS} = 90 Hz. (τ_p, τ_d) steps were (1 μs, 1 μs) and (5 μs, 5 μs) for experimental and calculated SIMPSON plots, respectively. Experimental ^{119}Sn MAS NMR spectra of $Y_2Sn_2O_7$ were acquired at B_0 = 9.4 T at an MAS rate of 10 kHz. The ^{119}Sn spectra are: (c) under MP decoupling (ν_1^O= 35 kHz) with (τ_P, τ_d) = (50 μs, 80 μs) corresponding to the circle in (b); (d) with optimized CW decoupling (ν_1^O = 35 kHz), and (e) without decoupling. At these conditions, the adiabatic passage parameter α is 0.2.

Figure 7 shows experimental (Fig. 7a) and simulated (using SIMPSON) (Fig. 7b) two-dimensional contour plots of ^{119}Sn signal amplitude under ^{17}O MP decoupling, as a function of (τ_p, τ_d) values. In both experiment and simulation the MAS rate and decoupling RF field strength were 10 kHz and 35 kHz, respectively. Experiments have been performed on $Y_2Sn_2O_7$, and plots show the peak height of the signal at –582.5 ppm. Figs. 6c, 6d and 6e show experimental ^{119}Sn MAS NMR spectra, acquired using ^{17}O MP decoupling (ν_1^O = 35 kHz) at τ_p and τ_d corresponding to the circle in Fig. 7b (Fig. 7c), under optimized CW decoupling at ν_1^{Al} = 35 kHz (Fig. 7d) and without decoupling (Fig. 7e).

The contour plot (Fig. 7b) for simulated data was generated using the spin system parameters extracted from the published available data and fits of the ^{119}Sn MAS NMR spectra (Fig. 7c to 7e, and [33]): C_Q = 4 MHz, D_{IS} = –680 Hz, J = 90 Hz (see supplementary information). This plot shows regions of good MP decoupling efficiency areas close to the rotor synchronization condition, for τ_p slightly smaller than τ_d. The (τ_p, τ_d) pair of (50 µs, 80 µs) corresponding to the circle in Fig. 7b, was used to acquire the ^{17}O MP decoupled spectrum.

An attempted fit (in red) of the complex lineshape of the ^{119}Sn MAS NMR spectrum is proposed in Fig. 6SI on the basis of J-couplings, considering a three component signal (a "singlet" component corresponding to uncoupled ^{119}Sn species in agreement with the pyrochlore structure of $Y_2Sn_2O_7$ described by Matteucci *et al.*[33–35] (purple), a doublet component corresponding to Sn experiencing a ^{119}Sn-^{117}Sn ^{2}J coupling of 180 Hz (green), and 11 line multiplet corresponding to Sn experiencing a ^{1}J coupling to two ^{17}O of 92 Hz (grey)). This tentative decomposition is by no means unambiguous, but was useful to point out the multiplet rising from the J coupling between ^{119}Sn and ^{17}O. The exact interpretation of the obtained ^{119}Sn NMR lineshape would probably require additional experiments at multiple fields.

As shown in Fig. 7d, the application of ^{17}O CW decoupling partly suppresses the component of the lineshape due to the coupling with the oxygens. Although the spectrum is narrowed using this approach, the effect of scalar decoupling is more impressive on the MP decoupled spectrum (Fig. 7c). Indeed, the linewidth is smaller due to an efficient scalar decoupling, which suppresses the multiplet ^{119}Sn-^{17}O component, even though the ^{119}Sn lineshape is still affected by the ^{119}Sn-^{117}Sn scalar coupling.

4. Conclusion

In the present article, we propose a guideline for the choice of experimental and instrumental parameters for MP decoupling of half-integer quadrupolar nuclei during the acquisition of spectra of nuclei with spin I = ½, in the case of a moderate heteronuclear dipolar interaction. This case is commonly encountered in inorganic materials when studying nuclei with relatively low γ (i.e., not ^{1}H or ^{19}F) that are coupled to each other. We have not treated this less common case where a large dipolar and a large quadrupolar coupling are present (direct ^{1}H-^{27}Al bonding for example). The evaluation of the decoupling efficiency was first evaluated with a numerical approach and confirmed experimentally for various half-integer quadrupolar nuclei (*e.g.*, I = 5/2 (^{17}O), 7/2 (^{51}V) and 9/2 (^{93}Nb)) coupled to nuclei with spin I = ½.

We have shown that the MP decoupling scheme is characterized by a pulse length (τ_p) and an interpulse delay (τ_d), values that need to be carefully chosen, as efficiency can vary quite considerably. This efficiency also depends on the instrumental parameters (*e.g.*, decoupling RF field strength, MAS rate) and intrinsic parameters of the material under study (*e.g.* heteronuclear dipolar and scalar interaction, quadrupolar coupling). We have considered three regimes (named as slow, fast and intermediate as a function of adiabatic passage

parameter value), and for each of them typical regions of efficient decoupling have been determined in terms of the values of τ_p and τ_d.

In all cases, the decoupling RF field strength should be chosen to be the highest possible, as this results in better decoupling efficiency. The MAS rate should be chosen to be reasonably high, removing the broadening due to the chemical shift anisotropy, in addition to a rotor-period τ_r of the order of >10 µs (*e.g* a MAS rate up to 100 kHz). This results in a broad region of efficient decoupling and ensures that the choice of (τ_p, τ_d) be less restricted.". However, high spinning rates, where the rotor period becomes of the the same order as the pulse length, should be avoided. As matter of fact, setting a very high spinning rate would imply that the regions of rotor-synchronization conditions (for instance $0.5\tau_r$, τ_r or $1.5\tau_r$) would be close from one another, so difficult to avoid. This would lead to a very picky choice of τ_p and τ_d away. For instance, if MAS rate is 150 kHz, then τ_r = 6.7 µs, 0.5 τ_r = 3.3 µs).

The optimal MP decoupling should be obtained following three main steps. Firstly, the rotor synchronized condition should always be avoiding. Secondly, one should validate or eliminate the extreme regime condition (α<0.05 and α>2-3). As a matter of fact, when α < 0.05 (sudden passage regime), long pulse lengths τ_p, much larger than interpulse delays τ_d, are chosen. Sometimes, CW decoupling can as well be used.

When α > 2-3 (adiabatic regime), one should use small τ_p compared to interpulse delay. Finally, if the regime is intermediate ($\alpha \in$ [0.1 ; 2-3]), τ_p and τ_p are quite close, and one might probe a few (τ_p; τ_d) pair chosen on either side of the rotor synchronized condition, to determine the best τ_p/τ_d ratio to choose in order to have the best MP decoupling efficiency possible.

To summarize, we have studied in detail the influence of experimental conditions and the parameters intrinsic to the material on the efficiency of MP decoupling efficiency for NMR observation of nuclei with spin I = ½ coupled to half-integer quadrupolar nuclei. The decoupling efficiency was investigated as a function of the decoupling RF field, MAS rate, and the magnitude of the heteronuclear interactions and the quadrupolar coupling constant of the remote spin. The consideration of simulated and experimental data for a variety of spin systems helped a series of general, time-saving guidelines to be proposed, designed to expediate experimental implementation of MP schemes. Heternonuclear interactions with proximate quadrupolar spins can limit the resolution in NMR spectra of spin I = ½ nuclei, even under MAS conditions. Improving this resolution, enabling the extraction of more accurate site specific information, will be a vital step for the future structural characterization of complex materials.

Acknowledgment
This work benefited from a grant from Agence Nationale de la Recherche (ANR MOSAIC 13-BS08-0018-01).

References

[1] A.L. Bloom, J.N. Shoolery, Effects of Perturbing Radiofrequency Fields on Nuclear Spin Coupling, Phys. Rev. 97 (1955) 1261–1265. doi:10.1103/PhysRev.97.1261.

[2] A.E. Bennett, C.M. Rienstra, M. Auger, K.V. Lakshmi, R.G. Griffin, Heteronuclear decoupling in rotating solids, J. Chem. Phys. 103 (1995) 6951–6958. doi:10.1063/1.470372.

[3] A. Detken, E.H. Hardy, M. Ernst, B.H. Meier, Simple and efficient decoupling in magic-angle spinning solid-state NMR: the XiX scheme, Chem. Phys. Lett. 356 (2002) 298–304. doi:10.1016/S0009-2614(02)00335-4.

[4] A. Equbal, M. Leskes, N.C. Nielsen, P.K. Madhu, S. Vega, Relative merits of r CW A and XiX heteronuclear spin decoupling in solid-state magic-angle-spinning NMR spectroscopy: A bimodal Floquet analysis, J. Magn. Reson. 263 (2016) 55–64. doi:10.1016/j.jmr.2015.12.019.

[5] B.M. Fung, A.K. Khitrin, K. Ermolaev, An Improved Broadband Decoupling Sequence for Liquid Crystals and Solids, J. Magn. Reson. 142 (2000) 97–101. doi:10.1006/jmre.1999.1896.

[6] R.S. Thakur, N.D. Kurur, P.K. Madhu, Swept-frequency two-pulse phase modulation for heteronuclear dipolar decoupling in solid-state NMR, Chem. Phys. Lett. 426 (2006) 459–463. doi:10.1016/j.cplett.2006.06.007.

[7] M. Weingarth, P. Tekely, G. Bodenhausen, Efficient heteronuclear decoupling by quenching rotary resonance in solid-state NMR, Chem. Phys. Lett. 466 (2008) 247–251. doi:10.1016/j.cplett.2008.10.041.

[8] A. Equbal, S. Paul, V.S. Mithu, P.K. Madhu, N.C. Nielsen, Efficient heteronuclear decoupling in MAS solid-state NMR using non-rotor-synchronized rCW irradiation, J. Magn. Reson. 246 (2014) 104–109. doi:10.1016/j.jmr.2014.07.006.

[9] K. Sharma, P.K. Madhu, V. Agarwal, Systematic evaluation of heteronuclear spin decoupling in solid-state NMR at the rotary-resonance conditions in the regime of fast magic-angle spinning, J. Magn. Reson. 270 (2016) 136–141. doi:10.1016/j.jmr.2016.07.007.

[10] V. Agarwal, T. Tuherm, A. Reinhold, J. Past, A. Samoson, M. Ernst, B.H. Meier, Amplitude-modulated low-power decoupling sequences for fast magic-angle spinning NMR, Chem. Phys. Lett. 583 (2013) 1–7. doi:10.1016/j.cplett.2013.07.073.

[11] G. De Paëpe, P. Hodgkinson, L. Emsley, Improved heteronuclear decoupling schemes for solid-state magic angle spinning NMR by direct spectral optimization, Chem. Phys. Lett. 376 (2003) 259–267. doi:10.1016/S0009-2614(03)00966-7.

[12] K. Riedel, J. Leppert, O. Ohlenschläger, M. Görlach, R. Ramachandran, Heteronuclear decoupling in rotating solids via symmetry-based adiabatic RF pulse schemes, Chem. Phys. Lett. 395 (2004) 356–361. doi:10.1016/j.cplett.2004.07.106.

[13] P. Hodgkinson, Heteronuclear decoupling in the NMR of solids, Prog. Nucl. Magn. Reson. Spectrosc. 46 (2005) 197–222. doi:10.1016/j.pnmrs.2005.04.002.

[14] P.K. Madhu, Heteronuclear Spin Decoupling in Solid-State Nuclear Magnetic Resonance: Overview and Outlook, Isr. J. Chem. 54 (2014) 25–38. doi:10.1002/ijch.201300097.

[15] S. Paul, N.D. Kurur, P.K. Madhu, On the choice of heteronuclear dipolar decoupling scheme in solid-state NMR, J. Magn. Reson. 207 (2010) 140–148. doi:10.1016/j.jmr.2010.08.023.

[16] L. Delevoye, J. Trébosc, Z. Gan, L. Montagne, J.-P. Amoureux, Resolution enhancement using a new multiple-pulse decoupling sequence for quadrupolar nuclei, J. Magn. Reson. 186 (2007) 94–99. doi:10.1016/j.jmr.2007.01.018.

[17] H.-M. Kao, K.-H. Lii, The First Observation of Heteronuclear Two-Bond J-Coupling in the Solid State: Crystal Structure and Solid-State NMR Spectroscopy of Rb4(NbO)2(Si8O21), Inorg. Chem. 41 (2002) 5644–5646. doi:10.1021/ic0204373.

[18] L.-S. Du, R.W. Schurko, K.H. Lim, C.P. Grey, A Solid-State ^{93}Nb and ^{19}F NMR Spectroscopy and X-ray Diffraction Study of Potassium Heptafluoroniobate(V): Characterization of ^{93}Nb, ^{19}F Coupling, and Fluorine Motion, J. Phys. Chem. A. 105 (2001) 760–768. doi:10.1021/jp0032006.

[19] L. Delevoye, C. Fernandez, C.M. Morais, J.-P. Amoureux, V. Montouillout, J. Rocha, Double-Resonance Decoupling for Resolution Enhancement of ^{31}P Solid-State MAS and ^{27}Al $\rightarrow^{31}$P MQHETCOR NMR, Solid State Nucl. Magn. Reson. 22 (2002) 501–512. doi:10.1006/snmr.2002.0080.

[20] G. Girard, F. Vasconcelos, L. Montagne, L. Delevoye, ^{31}P MAS NMR spectroscopy with ^{93}Nb decoupling and DFT calculations: A structural characterization of defects in a niobium-phosphate phase, Solid State Nucl. Magn. Reson. 84 (2017) 210–215. doi:10.1016/j.ssnmr.2017.05.003.

[21] E. Mazoyer, J. Trébosc, A. Baudouin, O. Boyron, J. Pelletier, J.-M. Basset, M.J. Vitorino, C.P. Nicholas, R.M. Gauvin, M. Taoufik, L. Delevoye, Heteronuclear NMR Correlations To Probe the Local Structure of Catalytically Active Surface Aluminum Hydride Species on γ-Alumina, Angew. Chem. Int. Ed. 49 (2010) 9854–9858. doi:10.1002/anie.201004310.

[22] N.F. Dummer, J.K. Bartley, G.J. Hutchings, Vanadium Phosphate Materials as Selective Oxidation Catalysts, in: Adv. Catal. Vol 54, 2011: pp. 189–247.

[23] R.L. Harlow, Z.G. Li, N. Herron, H.S. Horowitz, E.M. McCarron, J.W. jr Richardson, B.H. Toby, The crystal structure of the gamma phase of vanadyl phosphate, gamma-$VOPO_4$, solved and refined using both synchrotron and neutron powder diffraction data, ICSD Priv. Commun. (2005).

[24] A. Fernandes, R.F. Moran, S. Sneddon, D.M. Dawson, D. McKay, G.P.M. Bignami, F. Blanc, K.R. Whittle, S.E. Ashbrook, ^{17}O solid-state NMR spectroscopy of $A_2B_2O_7$ oxides: quantitative isotopic enrichment and spectral acquisition?, RSC Adv. 8 (2018) 7089–7101. doi:10.1039/C8RA00596F.

[25] S.E. Ashbrook, K.R. Whittle, G.R. Lumpkin, I. Farnan, ^{89}Y Magic-Angle Spinning NMR of $Y_2Ti_{2-x}Sn_xO_7$ Pyrochlores, J. Phys. Chem. B. 110 (2006) 10358–10364. doi:10.1021/jp060844q.

[26] M. Bak, J.T. Rasmussen, N.C. Nielsen, SIMPSON: A General Simulation Program for Solid-State NMR Spectroscopy, J. Magn. Reson. 147 (2000) 296–330. doi:10.1006/jmre.2000.2179.

[27] R. Siegel, N. Dupré, M. Quarton, J. Hirschinger, ^{51}V magic angle spinning NMR in $VOPO_4$ phases, Magn. Reson. Chem. 42 (2004) 1022–1026. doi:10.1002/mrc.1485.

[28] O.B. Lapina, D.F. Khabibulin, A.A. Shubin, V.V. Terskikh, Practical aspects of ^{51}V and ^{93}Nb solid-state NMR spectroscopy and applications to oxide materials, Prog. Nucl. Magn. Reson. Spectrosc. 53 (2008) 128–191. doi:10.1016/j.pnmrs.2007.12.001.

[29] L. Truflandier, Détermination de paramètres RMN par la théorie de la fonctionnelle de la densité : Application aux éléments 3d en RMN de l'état solide, Université de Nantes, 2007.

[30] A.J. Vega, MAS NMR Spin Locking of Half-Integer Quadrupolar Nuclei, Journal of Magnetic Resonance. 96 (1992) 50–68.

[31] C.P. Grey, A.J. Vega, Determination of the quadrupole coupling constant of the invisible aluminum spins in zeolite HY with ^{1}H/^{27}Al TRAPDOR NMR, J. Am. Chem. Soc. 117 (1995) 8232–8242.

[32] J.M. Longo, P. Kierkegaard, The crystal structure of $NbOPO_4$, Acta Chemica Scandinavica. 20 (1966) 72–78.
[33] F. Matteucci, G. Cruciani, M. Dondi, G. Baldi, A. Barzanti, Crystal structural and optical properties of Cr-doped $Y_2Ti_2O_7$ and $Y_2Sn_2O_7$ pyrochlores, Acta Mater. 55 (2007) 2229–2238. doi:10.1016/j.actamat.2006.11.008.